Stability, composition and properties of Li_2FeSiO_4 surfaces studied by DFT

N. G. Hörmann

Helmholtz Institute Ulm (HIU) Electrochemical Energy Storage, Albert-Einstein-Allee 11, 89069 Ulm/Germany

A. Groß

Helmholtz Institute Ulm (HIU) Electrochemical Energy Storage,
Albert-Einstein-Allee 11, 89069 Ulm/Germany and
Ulm University, Institute of Theoretical Chemistry, Albert-Einstein-Allee 11, 89069 Ulm/Germany

(Dated: April 18, 2013)

Surface structures and energies of the $Pmn2_1$ polymorph of the electrode material Li_2FeSiO_4 are studied by first-principles calculations using density functional theory. In total 29 surface terminations of stoichiometric *polar* and *non-polar* slabs were studied. These surfaces were preselected by energy estimation via a model that accounts for bond cutting and additionally for polarity compensation in the case of *polar* surfaces. The model provides a way to quantify the most important contributions to the surface energy. Furthermore, we analyse the relaxation of surface atoms statistically. This clearly shows that SiO_4 tetrahedra are rather rigid whereas the local environment of Fe and Li can change strongly under relaxation near the surface. We furthermore compare results obtained by GGA and GGA+U exchange correlation functionals. Thus we estimate the thermodynamic equilibrium shape of Li_2FeSiO_4 by the Wulff construction scheme for stoichiometric surfaces obtaining crystallites that are terminated by {110}, {010}, and {001} surfaces.

I. INTRODUCTION

Li_2FeSiO_4 is a promising new electrode material for Lithium ion batteries, due to the abundance, low cost and safety of the elemental components. Furthermore, it exhibits partly superior properties compared to $LiFePO_4$, such as better electronic conductivity and higher theoretical capacity[1], as in principle two Li ions per formula unit can be extracted or stored. The theoretical energy density of up to 300 mAh/g [2] has however not been realized in experiment. The extraction of the second Li works on the Fe^{3+}/Fe^{4+} redox couple which lead to extraction voltages beyond the stability of common electrolytes and instabilities of the structure, also for other transition metal ions [3, 4]. Experimental and theoretical studies on Li_2FeSiO_4 have found stable structures where the cations are located in the tetrahedral interstitials of a nearly hexagonally close packed framework of oxygen atoms [1, 5–8]. Depending on the crystal structure, the Li ions in transition metal silicates can either be arranged in layers [9], along lines or in a three-dimensional matrix. Thus ion conduction can be strongly anisotropic [10, 11]. The most common polymorph however crystallizes in the orthorhombic space group $Pmn2_1$ (see Fig. 1) which also first-principles calculations find to be the most stable polymorph [9, 12–15].

Though extensive experimental and theoretical studies have dealt with the properties of transition metal silicate materials in the bulk phase, few investigations have concentrated on surface properties and their relevance to electrode performance. The limited electronic and ionic conductivity of oxides however necessitates utilisation of nano-sized electrode particles rendering surface properties and processes especially important during cell oper-

ations. Indeed Li extraction voltages of Li situated at the surface can be very different from bulk, and diffusion through the surface can have decisive impact on the rate capability [16–18]. Furthermore, surface properties like energies of adsorption and of diffusion barriers are important in understanding crystal growth. Theoretical studies addressing these properties might help understand and optimize synthesis.

In this work, we determine the most probable and stable surface structures as a first step towards modeling surface processes in $Pmn2_1$ Li_2FeSiO_4. We present results of density functional theory (DFT) calculations of surface energies of Li_2FeSiO_4. As high resolution surface structure investigations by STM are hindered due to the low conductivity of the semiconductor-like ionic compound, first-principles calculations seem a straightforward route to determine the most important surfaces. By these calculations we determine the equilibrium shape of the crystal using the Wulff construction scheme. It is necessary to take into account a rather large selection of surfaces, in order to ensure having considered all low-energy surfaces contributing to the Wulff shape. We perform calculations on 29 different low-index surfaces. These surfaces were preselected by energy estimation via a model that accounts for bond cutting and additionally for polarity compensation in the case of polar surfaces. We analyse in detail the different energetic contributions of the surface energy for this specific compound and show that a combination of ionic and covalent bonds can reasonably describe the energetic behavior.

Furthermore we perform a statistical analysis of the relaxation behavior on the 29 surfaces. Also here we find clear signatures of non-homogenous bonds, i.e. rather strong, directional, covalent Si-O bonds and weaker, less-

directional, ionic bonds for Fe-O and Li-O. Finally we compare surface energies and Wulff shapes obtained by GGA and GGA+U exchange correlation functionals.

II. THEORY

A. Surface free energy

The surface energy γ_λ for surface λ is defined as the difference in energy of a semi-infinite solid that exhibits a surface and the energy of the respective half-space of the bulk material. As most calculations on solids are performed with periodic boundary conditions (PBC), the equivalent scenario is obtained by comparing the energy of (reasonably thick) slabs and respective bulk volumes. Obviously surface energies need to be positive for the bulk to be stable against decomposition. For nanosized materials the surface energy can indeed be a driving force for crystallyte morphologies and even phase stability, as bulk and surface contributions scale differently with the size of the crystal. The minimum total energy shape can be determined by the Wulff construction. Thermodynamic considerations, however, have to take into account the externally controlled variables. In experiment, the relevant variables are typically temperature, pressure and concentrations of the surrounding gas, liquid or bulk phase. Therefore it is required to consider surface *free* energies, determined by the difference in Gibbs free energies G of bulk and surface containing bulk, with:

$$G = \sum_i N_i \mu_i = U + pV - TS_{conf} + F_{vib} + F_{mag} \quad (1)$$

The surface (slab) is assumed in thermodynamic equilibrium with the bulk as well as with the environment characterized by temperature T, chemical potentials μ_i and partial pressures p_i. The surface free energy is then given by the difference of the slab's Gibbs free energy G_λ and the value for the respective individual atoms:

$$\gamma_\lambda(T, p_i, \mu_i) = \frac{G_\lambda(\{N_i^\lambda\}) - \sum_i N_i^\lambda \mu_i}{2A(\lambda)} \quad (2)$$

$$= \frac{1}{2A(\lambda)} \left(\Delta G_\lambda - \sum_i \Delta N_i^\lambda \mu_i(T, p_i) \right) \quad (3)$$

with $\Delta G_\lambda = G_\lambda(\{N_i^\lambda\}) - G_{bulk}(\{N_i\})$
and $\Delta N_i^\lambda = N_i^\lambda - N_i$

In this definition, we relate the total Gibbs free energy difference to both surfaces of the considered slab ($\frac{1}{2A}$), which is, however, not done consistently in literature. For symmetric slabs we obtain the surface energy of that very surface, for assymmetric slabs, we obtain the average surface energy of both surfaces. In fact it is possible to determine local energy densities [19], which allow an unambiguous determination of surface energies also for asymmetric slabs but this approach was not applied here.

Equation 3 indicates that for stoichiometric slabs, there is no dependence on the chemical potentials μ_i of the constituents as the bulk reference cell can be chosen such that $\Delta N_i^\lambda = 0$. In case of non-stoichiometric slabs, or surfaces containing adatoms the surface energy becomes a function of the chemical potential and of the number of the additional atoms. Thermodynamic considerations can be used to limit the reasonable range of accessible chemical potentials, and stable surface compositions can e.g. be analysed as a function of temperature, partial pressures etc. (see e.g. Refs. 20, 21).

In principle electronic, vibrational, magnetic and configurational degrees of freedom can play a role, where all necessary information can in principle be derived from the Hamiltonian describing the system. For a stoichiometric slab the number of vibrations will not be changed as compared to bulk and surface phonon energies will be in the energetic range of the bulk. Thus vibrational contributions ΔF_{vib} largely cancel out and can be neglected. Contributions for surface gas equilibrium are discussed extensively in Ref. 22. Magnetic effects (ΔF_{mag}) are not important in the system considered here, but in principle they require special attention (see e.g. Ref. 23). Electronic excitations are not important either in ionic materials. We also do not expect any major contributions due to configurational entropy S_{conf} for stoichiometric surfaces due to the rigidity of bonds; for Li_xFeSiO_4 (x≤2) they mainly cancel. Thus in our case, equation 3 reduces to a simple difference in ground state inner energies, which we calculate by DFT:

$$\gamma_\lambda = \frac{E_\lambda^{tot}(\{N_i\}) - E_{bulk}^{tot}(\{N_i\})}{2A(\lambda)} \quad (4)$$

In this study we are primarily interested in understanding basic surface energy trends and finding the most stable surfaces for Li_2FeSiO_4 ($Pmn2_1$). As there are no prior information on stable surface structures, we considered only stoichiometric surfaces. It should be noted here that the unit cell contains 16 atoms of four different elements which leads to a enormous variety of possible surface terminations, compositions and adsorption sites even for considering only one surface normal (e.g. [001]). Having said this, it becomes obvious that even taking only stoichiometric slabs with clean, unreconstructed, (1x1) surfaces into account still not limits the possible surfaces to a reasonable set. Furthermore high index surfaces as e.g. (230), show unexpectedly regular structures which indicate rather moderate surface energies even for higher Miller indices. Considering the considerably high computational cost of DFT calculations, there is still a need for approximate, numerically more efficient schemes that are adjusted to reproduce and interpolate results of DFT calculations [24]. Therefore, in order to be able to still address a reasonable number of different surface structures, we have employed an approximate model to estimate surface energies that accounts for bond cutting and polarity compensation for polar surfaces. This model is described in the next section.

B. Models for the surface free energy

The stability of surfaces can be estimated by evaluation of the number of broken bonds per unit area, electrostatic considerations or electron counting rules [25]. They originate mainly from the results of two extreme models: Purely covalently or purely ionically bonded materials.

For covalent materials the energy increase due to surface λ is assumed to be proportional to the number of cutted bonds per area:

$$\gamma_\lambda \cdot 2A(\lambda) = \sum_{i,j} E_{i,j} \cdot n_{i,j}(\lambda) \qquad (5)$$

where i describes the cation and j the coordination. In our case, this is sufficient as every cation is 4-fold coordinated to oxygen in bulk. $E_{i,j}$ is zero for atoms coordinated as in bulk, and takes some positive value for undercoordinated surface atoms. Surface creation is viewed as a process of *local* bond breaking, i.e. only including nearest neighbor forces/bonds.

On the other hand, in the ionic picture, surface creation is interpreted as substituting the infinite Madelung sum by a semi-infinite one, thus as a change of the *long-range* Coulombic interaction. General considerations showed that slabs with finite perpendicular dipole-moment - so-called *polar* surfaces - implicate diverging electrostatic energies for infinitely thick slabs[26]; they are often classified according to Tasker[27]. This approach is appealing because of its simplicity, however, there are problematic cases [25, 28–30]: *polar* surfaces are often not properly described and exist with surface energies that are unexpectedly moderate. Furthermore, the ambiguity in decomposing the continous charge density on seperate ionic cores, leads to an ambiguity in the definition of polar surfaces. Still, recently some progress has been made in this context [31].

Both approaches have in common that they rely only on bulk properties and that slabs can be analysed with them prior to calculations. It should be noted, however, that neither approach includes or predicts effects due to relaxation.

C. Selection procedure of considered surfaces

As already mentioned, the complexity of the unit cell leads to an enormous variety of possible surface structures. In order to restrict the search, we concentrated on planar cuts through the crystal, (1x1) surface cells without reconstructions and stoichiometric slabs.

In order to find the low energy surfaces by ab initio calculations we need a method that enables quick and rough estimation of surface energies. This furthermore makes the selection procedure of considered slabs less dependent on our possibly biased intuition.

We used the following scheme:

1. Calculation of surface energies on an initial collection of slabs by DFT.

2. Determination of the $E_{i,j}$ parameters of eq. 5 by fitting.

3. Prediction of surface energies according to eq. 5 on a large selection of slabs.

4. Recalculation of predicted low energy surface energies by DFT.

The unit cell of $Pmn2_1$ Li_2FeSiO_4 has no center of inversion, therefore also *polar* surfaces need to be considered for the Wulff construction. No electrostatic interactions are included to this point in our surface energy prediction. We will come back to that later. Essentially the same routine was applied by Wang et al. in their investigation of $LiFePO_4$ surfaces [16]. However, further restrictions had been imposed in this work, such as not allowing for P-O bond cutting and excluding polar surfaces completely from the selection of low energy surfaces, as also done by others (see, e.g., Ref. 32). We do not impose any of these restrictions and solely rely on the predictions of eq. 5. This enables automation as soon as step 2 is finished. Construction of slabs with all possible surface terminations and for all possible (hkl) can be formulated as linear algebra operations on the bulk unit cell. We have implemented corresponding operations in a *python* program, which heavily relies on the perfectly written and documented object-oriented structure manipulation toolkit *pymatgen* [33] of the Ceder group.

D. DFT calculations

Total energy calculations have been performed within periodic DFT using the Vienna Ab initio Simulation Package (VASP) [34, 35]. We used the generalized gradient approximation (GGA) of Perdew-Burke-Enzerhof (PBE)[36] as exchange correlation functional as well as GGA+U in the rotationally invariant form[37]. GGA calculations are known to describe structures and processes at surfaces, in particular metal surfaces [38, 39], but also Li ion battery electrode surfaces [40, 41], quite reliably, however, GGA+U can improve results of total energy calculation as GGA is known to fail, especially in oxide systems, in predicting certain features of correlated d electrons correctly [42–44] mainly due to self-interaction errors. Most Li ion electrode materials in fact need to be described by GGA+U in order to obtain reasonable values for Lithium extraction voltages [45, 46]. The Hubbard U parameter can in principle be determined self-consistently. We have set U = 5 eV and I = 1 eV[3, 9, 45] for Fe, noting that differences of 0.5 eV do hardly matter [16]. The core electrons are represented by projector augmented wave (PAW) pseudopotentials [47] as supplied in VASP [48]. The Brillouin zone integration is performed on a 5x5x5 Γ-centered k-point grid for bulk.

Denser k-point grids have practically no influence on the total energy (1 meV/formula units). The plane wave cutoff was set to 600 eV, where the error is approximately 20 meV/formula unit $\approx$ 2.5 meV/atom.

A detailed convergence study revealed that errors in surface energy are smaller than 3 % with these parameters. It should be stressed here that we prefer a large ammount of considered surfaces to absolute accuracy in this study, as we presume that the proper surface selection has the largest influence on the validity of the predicted Wulff-shape. Furthermore the chosen parameters are well in line with other calculations on this system [3, 4, 9, 49–52]. The threshold for the electronic self consistent cycle is set to 10^{-4} eV; ionic relaxation were stopped when forces were smaller than 0.01 eV/Å. Surface energies are determined from slab calculations in the supercell approach. The Γ-centered k-point mesh was changed to 5x5x1 and in case of large surface unit cells scaled appropriately (e.g. 3x5x1 for a (001)(2x1) surface unit cell). In cases of slow ionic convergence the force threshold was increased to 0.02 eV/Å. All slab calculations were performed with dipole correction [53–55] in order to remove the artificial electrostatic fields arising from asymmetric slabs in periodicity conditions.

Converged surface energy values were obtained for vaccum distances larger than $\approx$ 15 Å. Slab thicknesses ranged from 10 Å (high index surfaces)-40 Å (low index surfaces), reasonable convergence was typically achieved for thicknesses larger than 15 Å. We did not extrapolate the thickness dependence to infinity but rather used the average of values of thicker slabs, where energies did not vary more than 1 meV/Å.

For each surface all atoms up to 5 Å below the surfaces on both sides of the slab were allowed to relax. Reasonable convergence was obtained for these values ($\Delta\gamma < 0.5$ meV/Å^2). In several cases, especially for polar surfaces, calculations were also performed allowing all atoms to relax. The reason is that polar slabs are expected to have a non-vanishing macroscopic electric field throughout their interior, to which the ions will response by displacement. This displacement will not fall off with increasing distance from the surface, and corresponds to the dielectric response to the field (see section III C).

III.   RESULTS

The surface selection routine as described above was performed within standard GGA. The surface energy of the most interesting low energy surfaces was also calculated with the GGA+U approach. We subsequently compare the results of both methods.

A.   Results for bulk

The results obtained for bulk with GGA and GGA+U are summarized in table I. For each method, the en-
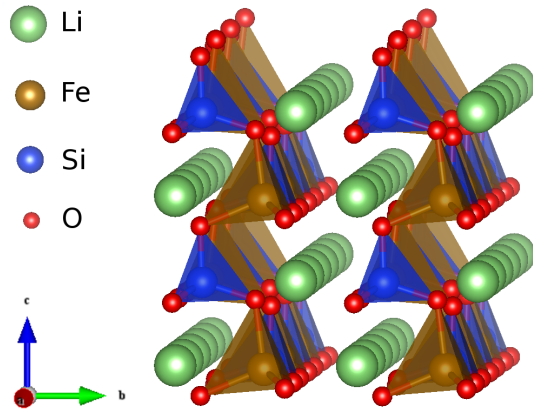

FIG. 1: Bulk structure of Pmn2$_1$ Li$_2$FeSiO$_4$ in a 2x2x2 supercell.

ergy volume dependence was determined and fitted with a Birch-Murnaghan equation of state. The equilibrium shape was determined from a subsequent run started at the fitted equilibrium volume where cell shape, volume and atoms were allowed to relax. No energetic difference was observed for runs with parallel and antiparallel spins on the two Fe 3d atoms. Nevertheless spin-polarized calculations are required as the Fe^{2+} 3d^6 electrons were found to prefer a high spin state of 4. For convenience d electrons on both Fe atoms were initialized in parallel spin configurations. Our values are in good agreement with published experimental and theoretical values. The first-principles determination of Lithium extraction voltages shall not be discussed here (see e.g. Ref. 45), nevertheless note the discrepancy between GGA and experiment, and the good agreement of GGA+U and experiment. The geometry of the bulk unit cell is displayed in Fig. 1, drawn with VESTA [56].

B.   Surface energies (GGA)

In order to evaluate the surface energies, we used a three-step approach.

TABLE I: Obtained bulk properties for the Pmn2$_1$ polymorph of Li$_2$FeSiO$_4$. Some published computational and experimental values are added for comparison. B$_0$ is the bulk modulus, Voltage the average extraction voltage for the first Li.

Reference	GGA This study	GGA+U This study	GGA 50	GGA+U 9	Exp. 14	Exp. 15
a (Å)	6.286	6.313	6.290	6.320	6.270	6.267
b (Å)	5.372	5.384	5.375	5.384	5.345	5.330
c (Å)	5.003	4.996	5.002	4.998	4.962	5.015
V$_0$ (Å^3)	169.0	169.8	169.08	170.05	166.3	167.5
Voltage (V)	2.59	3.12	2.6	3.12	3.13	3.10
B$_0$(eV/Å^3)	0.5390	0.5305				

STEP 1: Initially a selection of 13 surfaces of type {100}, {010}, {001}, {011}, {101}, {110}, {210}, or {120} was determined intuitively. 6 of them are *non-polar* and 7 *polar*. The bond cutting expressions for these surfaces have contributions from 8 different parameters $n_{i,j}$. Surface energies were calculated and the bond cutting expression of eq. 5 was fitted to the results. It it implicitely assumed that all changes due to relaxation and long-range effects such as electrostatic energy changes and electronic charge redistribution are in some way included in effective bond-cutting energy values $E_{i,j}$.

STEP 2: The fit was performed by minimizing the relative, squared deviation Δ:

$$\Delta = \sum_\lambda \left(1 - \frac{\sum_{i,j} E_{i,j} \cdot n_{i,j}(\lambda)}{\gamma_\lambda \cdot 2A(\lambda)} \right)^2 \quad (6)$$

Δ is chosen as the relative deviation in order to ensure that low energy surfaces have a heigher weight in the fit, as we are in fact interested in a good representation especially for potentially low energy surfaces. Analytical minimization of equation 6 by setting the partial derivatives to zero leads to an underdetermined system of equations, in other words, a matrix equation of the form $\mathbf{M}x = b$, with singular matrix $\mathbf{M}$. The reason is that only one surface contains singly coordinated Si and Fe, rendering an individual energy assignment ambiguous. A singular value decomposition of matrix $\mathbf{M}$ results in equal partitioning of the surface energy between Si and Fe. Leaving out either parameter from the fit will assign the whole energy to the remainder. The obtained fit parameters for the reduced 7 parameter model are summarized in Table II. The values in brackets are chosen intuitively for the subsequent surface energy predictions. As low energy surfaces are not expected to have neither singly coordinated Si nor Fe, this should not influence the predictive quality.

The sum of squares of residuals (RSS) is 10.6 %, which is a measure for the deviation of the fit. The fitted values coincide with what chemical intuition would suggest: that the bond breaking energy of the cation-O bonds are $E_{Si,j} > E_{Fe,j} > E_{Li,j}$ and larger for smaller coordination j. Bond breaking is most unfavorable for Si-O bonds. The determined value of ≈ 3.4 eV is, as expected, of the
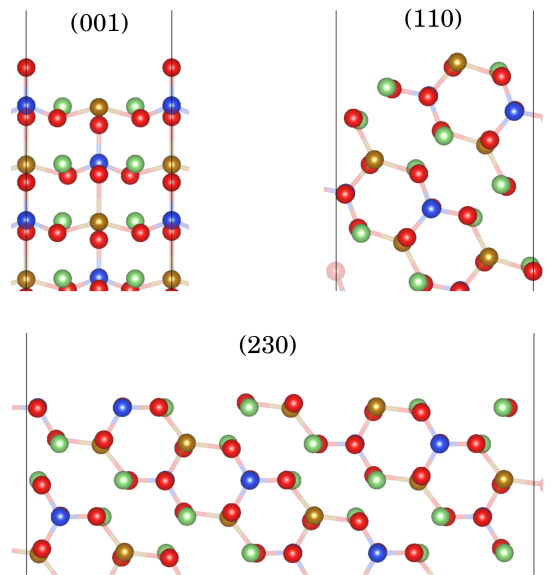

FIG. 2: Surface terminations of unrelaxed (001), (110) and (230) surfaces. In spite of the high index, the (230) termination exhibits a higher degree of order as compared to the (110) termination. Fe-O and Si-O bonds are indicated by sticks.

TABLE II: Surface energy contributions for undercoordinated surface atoms, as obtained from the fit. Values in parantheses are those which were chosen for surface energy predictions. Due to the limited number of surfaces, these cannot be assigned unambiguously.

$E_{i,j}$ (eV)		coordination		
		1	2	3
	Si	11.5318 (6.7659)[a]	4.5541	3.3554
element	Fe	(4.7659)[a]	2.5643	0.6082
	Li	(0)[a]	0.0218	0.3818

[a]Chosen parameters for energy prediction

order of the binding energy for the Si-O bond (≈ 4.6 eV) [57]. The energy scales also suggest that our accuracy is sufficient for predicting the most stable surfaces. Cutting the first Fe-O bond, which means reducing the coordination of Fe to be 3, seems to have no large influence on the surface energy, removing two bonds, however, has. Undercoordinated Li ions have no strong influence on the surface energetics, which should be expected for intercalation materials, as a small bond breaking energy of Li is related to Li extraction barriers and diffusivity. The obtained trend of Li to favor twofold over threefold coordinations is propably due to the limited number of surfaces and effects which are not included in equation 5.

STEP 3: The parameters from table II have now been used to predict surface energies for all possible stoichiometric terminations $\{\lambda(hkl)\}$ for all $\{hkl\}$ surfaces with $0 \leq h,k,l < 4$. These are 46 [hkl] directions and for each (hkl) ca. 10-15 possible surface terminations (including symmetry equivalent ones). For each surface (hkl) the lowest energy configuration $\lambda_{min}(hkl)$ was determined in the following way:

$$\lambda_{min}(hkl) = \begin{cases} \mathrm{argmin}\{\gamma_{\lambda^*(hkl)}\} & \text{if } \{\lambda^*(hkl)\} \neq \emptyset \\ \mathrm{argmin}\{\gamma_{\lambda(hkl)}\} & else \end{cases} \quad (7)$$

where $\{\gamma_{\lambda(hkl)}\}$ represents the set of surface energies derived from the set of surfaces $\{\lambda(hkl)\}$ and $\{\lambda^*(hkl)\} = \{\lambda(hkl)|\lambda(hkl) = \text{``non-polar''}\}$. So, if there is a non-empty set of cuts perpendicular to [hkl] that create non-polar (hkl) slabs, then only the minimum within this set is determined. Thereby, major, unreasonable predictions of low energy surfaces are suppressed and electrostatic

arguments somehow taken into account. Due to the reduced number of fitted surfaces, one might wonder about the accuracy of $E_{i,j}$ and the reliability of predicted low energy surfaces. We checked the robustness of our prediction method for low energy surfaces by varying the parameters $E_{i,j}$ by ±15%.

Then all surfaces of minimum surface energy were redetermined by the algorithm 7 for different parameter sets. In summary, for each direction [hkl] not more than three lowest surface energy terminations were found. The one with highest probability for given [hkl] corresponded always to the one obtained for the average parameters $\{E_{i,j}\}$ of table II. All low energy surface terminations are predicted with high "stability" (89%-100% occurence). This result suggests that the predictions with eq. 5 are not too sensitive to the $E_{i,j}$ parameters, which in effect justifies that we chose the underdetermined parameters intuitively, and did not increase slab numbers for fitting.

From the estimated low energy surfaces, 18 are indeed predicted to be lower in energy than the energetically 3rd most stable surface from the 13 <u>STEP 1</u> DFT calculations. In some cases planar cuts would not result in symmetric slabs although shuffling of one atom on its symmetry equivalent place on the other side of the slab would produce this. In these cases both terminations were calculated. As expected we found consistently lower energies for the symmetric slabs. In this way surface energies for 16 additional surface terminations have been calculated. Interestingly enough, we also find rather stable high index surfaces, as lower hkl indices are not necessarily connected to a more closed surface. This can e.g. be seen in Fig. 2, which shows the unrelaxed (001) ($\gamma = 60$ meV/Å^2), (110) ($\gamma = 32$ meV/Å^2) and (230) ($\gamma = 81$ meV/Å^2) surface terminations.

Thus the collection of investigated surfaces consists finally of 29. The surface energies are plotted in Fig. 3 discriminating between polar (squares) and non-polar surfaces (circles). It can be seen that non-polar surfaces tend to be quite well described with the local bond cutting model (except for one data point), whereas polar surfaces have rather drastic deviation. Furthermore polar surfaces have positive deviation from the model prediction and non-polar ones negative (except for two data points, see Fig. 3).

This suggests that indeed a non-negligible, non-local, electrostatic contribution is present for the investigated *polar* surfaces that obviously cannot be represented by the local bond cutting expression.

In order to prevent diverging electrostatic surface energies for thick *polar* slabs several charge compensation mechanisms have been discussed in literature [28]. We have derived a general approximate expression for the surface energy within the ionic model where charge transfer (= surface metallization) is viewed as the polarity compensating mechanism. For the derivation, see Ref. 58. We obtain for the electrostatic contribution γ^{es}:

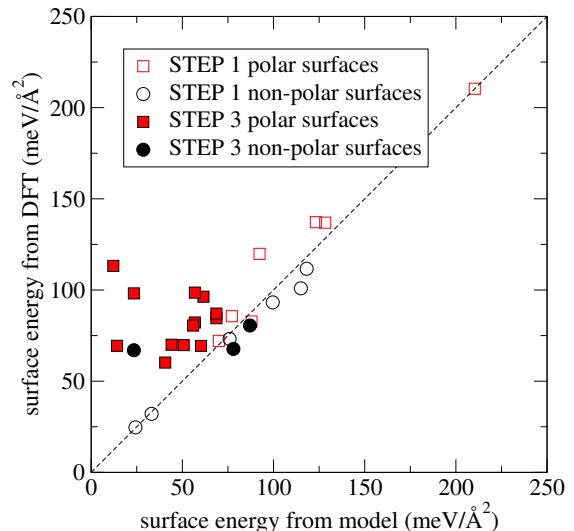$$\gamma^{es} \approx \frac{1}{2} E_G \sigma_0 \qquad (8)$$

FIG. 3: Comparison of DFT results for surface energies and the values obtained from the fitted bond cutting model. The diagonal is indicated by a dashed line. The predicted - STEP 3 - low energy surfaces whose surface energies were calculated by DFT are represented by filled symbols.

TABLE III: Ionic charges in Li$_2$FeSiO$_4$, according to oxidation state obtained by a Bader charge analysis of the DFT calculations.

element	Li	Fe	Si	O
q^{ox}/e	1	2	4	-2
q^{Bader}/e	0.85	1.27	3.11	-1.52
q^{Bader}/q^{ox}	0.85	0.64	0.78	0.76

with E_G related to the bandgap via $E_G = E_g/e$, and σ_0 to an effective surface charge, defined by the charge distribution in the slab unit cell of Volume V_0 and thickness d_0:

$$\sigma_0 = \frac{\int_{V_0} z\rho(\mathbf{r}) \; \mathrm{d}^3 r}{A d_0} = \sum_{z_i \in V_0} \sigma_i \frac{z_i}{d_0} \qquad (9)$$

$\rho(\mathbf{r})$ is the charge density of ionic, point-like charges. A Bader decomposition has been performed for bulk Li$_2$FeSiO$_4$ which results in local ionic charges as given in table III.

Due to the simplicity of the oxidation state approach and the similar fractional values q^{Bader}/q^{ox}, σ_0^{ox} shall from now on be simply referred to as σ_0 and taken as surface specific variable. This further circumvents any discussion about the appropriate approach to project the electronic charge density onto single atoms [59, 60].

As a result of these considerations we added a factor linear in σ_0 to the bond-breaking expression:
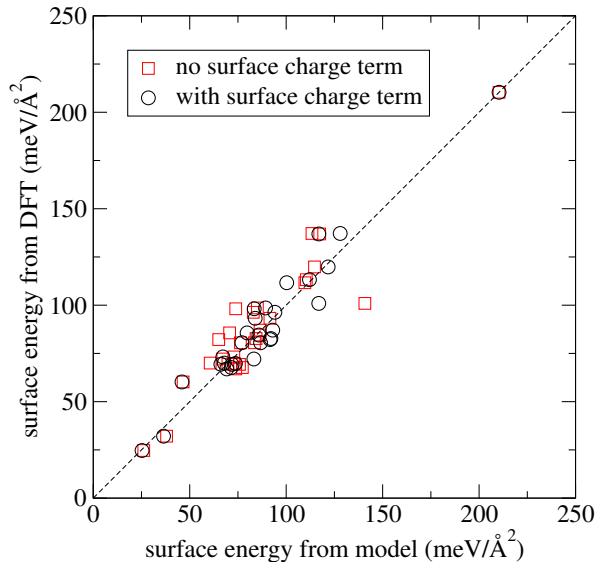
FIG. 4: Estimation of the accuracy of the used models. Results from the bond cutting model without surface charge term (eq. 5) are represented by red squares, results with surface charge term (eq. 10) by black circles.

$$\gamma_\lambda \;=\; \frac{\sum_{i,j} E_{i,j} \cdot n_{i,j}(\lambda)}{2A(\lambda)} + C \cdot \sigma_0(\lambda) \qquad (10)$$

We refitted the old (no surface charge contribution) and the new expression (with surface charge contribution) to the 29 surface energies obtained by DFT. The obtained parameters are given in table IV. The accuracies are drawn in Fig. 4.

In fact the average deviation with charge term (eq. 10) is improved by $\approx 30\%$ compared to setting C = 0 V (RSS is 0.497 without charge term, with charge term it is 0.251).

Furthermore the constant C obtained from the fit corresponds in size to what we expect theoretically. The bond-breaking terms are in a similar regime as obtained from the STEP 2 fit, and do slightly shift when the charge term is included. In fact the obtained values seem more reasonable as from the first fit on 12 surfaces. Our model inherently enables to separate and evaluate the size of

TABLE IV: Parameters $E_{i,j}$ and C, as obtained from fitting the models to the 29 surface energy values. Values in parantheses are those obtained from fitting the pure bond cutting expression corresponding to $C \equiv 0$ in Eq. 10.

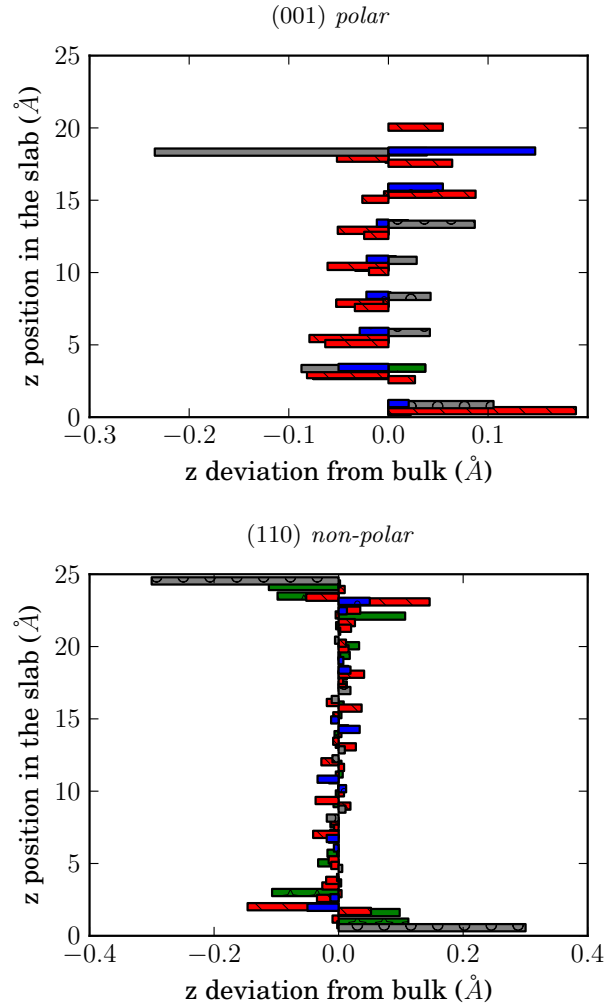| $E_{i,j}$ (eV)		coordination		
		1	2	3
element	Si	12.193 (12.294)	3.150 (4.070)	2.676 (2.965)
	Fe		1.835 (2.228)	0.712 (0.750)
	Li	2.361 (3.062)	1.147 (1.235)	0.398 (0.411)
C (V)		0.3831 (0.0000)		

FIG. 5: Relaxation of a *polar* (001) and *non-polar* (110) slab (surface terminations as in Fig. 2).Disentangling of specific relaxation behaviors is rendered complicated due to the complex crystal structure. Note however the non-vanishing relaxation in the center of the *polar* slab, which is testimony to the macroscopic electric field due to effective surface charges. Colors: Li: *green*; Fe: *grey*; Si: *blue*; O: *red.*

bond-breaking and electrostatic contributions.

C. Relaxation analysis (GGA)

Conventionally surface relaxations are discussed with respect to certain atomic layers, as e.g. surface layer spacings in metals [38]. Similarly binary compounds could be analysed e.g. by the relaxation of the sublattices. Often concepts of non-directional metallic or ionic bonds or directional covalent bonds help to understand equilibrium, low temperature surface structures. Ionic surfaces typically show rather small relaxation, if the structure is already close-packed[61].

In Li_2FeSiO_4 bonds cannot be classified uniformly due

to the 4 individual atom species. Furthermore, the complex crystal structure renders the definition and discussion of atomic layers somehow problematic. We exemplify the complex behavior in Fig. 5, which shows the relaxation in direction perpendicular to the slab surface for the (001) and (110) slabs, that correspond to the surfaces as depicted in Fig. 2. In general, most surfaces show an inward relaxation of undercoordinated surface atoms with some reaction of sub-surface atoms [62], however, relaxation is rather complex and different for different atomic species. Indeed different behavior can be seen for *polar* and *non-polar* slabs, as expected. *Non-polar* slabs show significantly faster decrease of atomic relaxation with distance from the surface (see Fig. 5). Due to the non-vanishing macroscopic field that extends across *polar* slabs, we find noticeable deviations from the atomic equilibrium positions even in the center of thick *polar* slabs. Indeed the response of cationic and anionic sub-lattices can be understood easily in well ordered binary materials, where the opposing relaxations of the sublattices effectively reduce the total dipole across the slab. Fig. 5 indicates, however, that the relaxation behavior in the case Li_2FeSiO_4 is slightly different, as e.g. the cations Si^{4+} and Fe^{2+} move in opposing directions. However, the behavior can be well understood when we discriminate not between the individual atom species but consider the crystal rather as composed of more complex subunits. The assumption that Si does not respond individually as Si^{4+}, but that it is rather the covalently bound SiO_4^{4-} subunit reestablishes the general understanding of relaxation behavior for the *polar* (001) surface: whereas O^{2-} and SiO_4^{4-} move towards the bottom of the slab, Fe^{2+} moves to the top (see Fig. 5), as consequence of the internal field.

This fact motivates to analyse relaxation by studying how the bonding situation changes during relaxation. Hence, instead of relaxation vectors or layer spacings we take a statistical analysis approach to understand how bonds to nearest neighbors change. As mentioned above, Li_2FeSiO_4 has a nearly close-packed oxygen matrix with cations sitting on tetrahedral interstitials. For bulk, each cation is surrounded by four oxygen atoms. The close connection to a tetrahedral arrangement can be seen from table V. The tetrahedra formed by the oxygen surrounded cations are close to perfect. Especially Si shows values that indicate rather low distortion from a perfectly symmetric tetrahedron.

Here we analyse surface relaxation by calculating the average bond lengths, angles and the standard deviations σ and comparing the values before and after relaxation. Bonds to neighboring atoms are established whenever the distance of the two atoms is smaller than 2.5 Å. This value is of course somehow arbitrary but motivated by bulk considerations. Spheres around cations in bulk with radiuses between 2.1 and 2.8 Å will have only the 4 next nearest oxygen neighbors inside. Therefore a cutoff radius in between these borders is chosen. The analysis has been performed on 28 surfaces, for each atom. Compar-
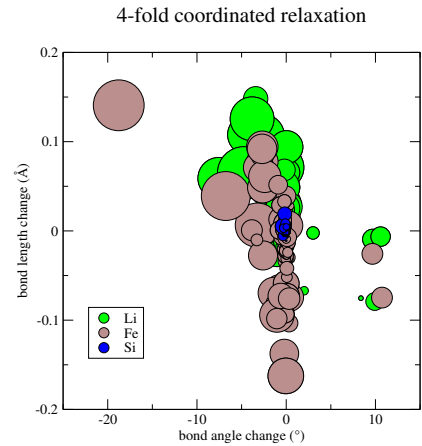

FIG. 6: Relaxation of 4-fold coordinated sub-surface atoms. The radius corresponds to the variation in the average bond length (see text).

ing directly the change of each bond length fails as atoms can change their coordination upon relaxation. Therefore only the difference in average value of bond length and angle were determined. Variances are added. Large variances (standard deviations) always indicate a deviation from a symmetric configuration (see Fig. 6).

To understand the behavior it is helpful to take a perfect tetrahedron as model. In general a reduction of bond length will obviously correspond to an inward movement of surface atoms, which is typically accompanied by an increase in bond-angle. Any asymmetry will increase the standard-deviation.

Following questions shall be adressed:

1. Is the relaxation behavior dependent on the coordination of the atom?

2. How differently do different species of atoms relax?

The relaxation behavior for the different coordinations for each cation is illustrated in Fig. 7.

For Li, rather large bond length variations are observed, even for four-fold-coordinated atoms. Furthermore, definite clustering is observed for undercoordinated surface atoms. Two-fold coordination results in stronger

TABLE V: Average bond lengths and angles for bulk Li_2FeSiO_4. A perfect tetrahedral arrangement would result in an angle $\approx 109.47°$ and standard deviations σ of 0.

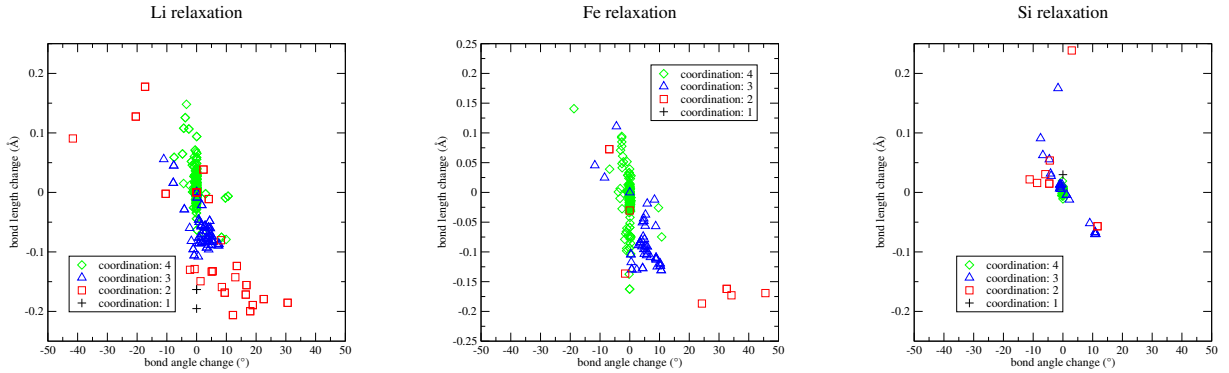| element	bond length (Å)	standard dev. (Å)	bond angle (°)	standard dev. (°)
Li	1.99	0.02	109.43	2.64
Fe	2.02	0.03	109.20	8.22
Si	1.66	0.00	109.46	0.94
O	1.91	0.15	109.05	7.5

FIG. 7: Change of local bond angles and bond lengths for the different cations and for different coordination numbers upon relaxation (4-fold ≡ sub-surface atoms).

relaxation towards the bulk than three-fold. The change of bond angles is significantly larger for two-fold coordinated Li than for three- and four-fold, and distributed rather homogeneously. As expected, bond lengths and angles are anticorrelated.

Although the statistical sample is smaller for the Fe atoms, similar results seem to hold for Fe. The bonds are rather flexible also for "bulk-like" 4-fold coordinated atoms. In average, two-fold coordination results in stronger bond length reduction than three-fold. Though bond-angle variations for 2-fold coordinated Fe are less homogeneous as compared to Li, and Fe seems to prefer larger bond angles.

In contrast to the two other cations, Si behaves differently. Firstly, the four-fold coordinated atoms show nearly no relaxation, in contrast to the other elements of Li_2FeSiO_4. A clear trend is observed for three-fold coordinated ions. Centered around (0,0), a nearly linear behavior with negative slope is observed, similar as expected. It seems that the relaxed SiO_x blocks in the surface are closer related to the tetrahedral-like original than in the case of Fe and Li. It can furthermore be observed that two-fold coordinated Si does not relax towards larger bond-angles and smaller distances as the other cations, but rather does the opposite.

In order to see the differences more clearly, we compare the behavior of the different four-fold sub-surface cations in Fig. 6. We hereby observe the response of bulk-like coordinated cations adjacent to a perturbation, the surface. The size of the circles corresponds to the square root of the sum of variances of bond lengths before and after relaxation. This corresponds to the standard deviation σ of the average bond length difference. A large radius is thus connected to a large deviation from the symmetric, tetrahedron-derived atom arrangement. Obviously Li and Fe are much more prone to changing their local atomic arrangement and relax e.g. to asymmetric bonding structures. We interpret this as a signature of covalent Si-O bonds derived from strongly directional sp^3

hybridized Si orbitals. This explains a) the nearly linear behavior in Fig. 7 for three fold coordinated Si and b) the extremely low values for the standard deviations in Fig. 6, which indicate relaxation that retains the tetrahedron derived symmetry. The other cations, on the other hand, show much lower directional bonds.

D. GGA vs. GGA+U

As stated above, several properties of transition metal oxides are described more properly by the GGA+U approach. Thus we have recalculated several low energy surfaces by GGA+U. In general, surface energies increase compared to the GGA values, as tabulated in table VI. This is true for polar and also non-polar surfaces. The low energy (010) surface only involves Li-O bond cutting and shows nearly no difference, an indicator that Li-O bonds are not strongly influenced by the GGA+U treatment of Fe d orbitals. In fact, this is in line with the element specific differences of the LDOS between GGA and GGA+U, which we will not discuss here further.

E. The Wulff shape

Because of our distinct selection procedure of low energy surfaces, we assume that all important stoichiometric low energy surfaces have been considered. This makes it possible to determine the Wulff shape of Li_2FeSiO_4 crystallites – the surface enclosing a fixed volume with

TABLE VI: Surface energies γ in meV/$Å^2$ of several surface terminations calculated by GGA and GGA+U

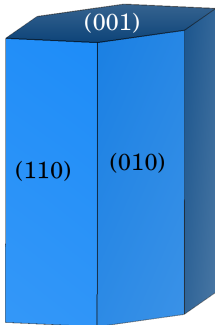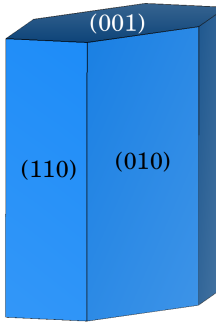| (hkl)	(010)	(110)	(001)	(100)**	(011)**	(010)*
GGA	24.7	32.1	60.2	67.0	69.4	113.2
GGA+U	25.4	39.1	68.1	76.7	81.7	137.2

least surface energy, and thus least total energy. In fact, only three of the considered 29 surfaces contribute to it: two non-polar surfaces (010) and (110) and one polar termination (001). The prismatic Wulff shapes are depicted in table VII as obtained from GGA and GGA+U surface energy values.The shapes are rather similar, only the relative contributions of (010) and (110) terminated surfaces change slightly.

F.   The low energy surfaces

The composition of the low energy surfaces is depicted in Fig. 8, where the bond cutting model parameters lead to an obvious interpretation of the observed structure: (010) and (110) surfaces are non-polar and thus have no large electrostatic energy energy contributions. It should be further noted that these two surfaces exhibit noticeably lower surface energy than all others (see Table VI). The stability is governed by the types and number of broken bonds.

- The (010) termination has only undercoordinated Li atoms at the surface, it corresponds to a cut through the Li double layer (see Fig. 1), and is the most stable of all stoichiometric surfaces (see Fig. 4 and Tables IV and VI).

- The (110) termination leaves SiO_4 tetrahedra intact and only produces undercoordinated Fe and Li at the surface. Although it looks rather open and corrugated, the low surface energy value can be understood considering the rather small bond cutting parameter for 3-fold coordinated Fe and Li (see table IV). The surface termination is depicted in Fig. 2 and 8.

TABLE VII: Comparison of the Wulff shape and the contributions of different surfaces as obtained from GGA and GGA+U calculations.

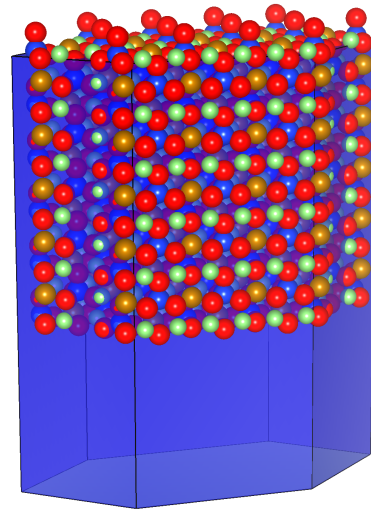| GGA	GGA+U
{010} : 28.14 %	{010} : 35.24 %
{110} : 52.13 %	{110} : 45.20 %
{001} : 19.73 %	{001} : 19.56 %

FIG. 8: Illustration of the atomic surface composition of the $Pmn2_1$ Li_2FeSiO_4 crystallite with equilibrium shape.

- The determined (001) surface is in a way special, as it avoids cutting through Si-O bonds and at the same time exhibits rather moderate effective surface charge (see Fig. 2 and 8). This should be compared to the (001) termination which cuts through the topmost Si-O bond, where the surface is however much less corrugated but exhibits a higher surface energy (72 meV/$Å^2$ instead of 60 meV/$Å^2$ for GGA). The depicted lowest energy (001) termination however exhibits unsaturated singly coordinated oxygen atoms that are of course very reactive. As a matter of fact, preliminary calculations indicate that for reasonable Li chemical potentials these will be saturated with Li and with the presented stoichiometric structure being stable for an applied voltage of $\gtrsim$ 1.2 V vs. Li/Li$^+$.

Here, however, we wanted to concentrate on stoichiometric surfaces, and show that a simple model as developed is helpful to understand the composition of low energy surfaces in complex oxides such as Li_2FeSiO_4. Any non-stoichiometric surface compositions, also of the other surfaces, need thorough investigation due to the variety of adsorption sites. We are addressing such structures at the moment.

IV.   CONCLUSION

We have studied the surface energies of different surface terminations of Li_2FeSiO_4, a promising material for battery electrodes. Because of the large variety of possible surface structures, simple models are helpful to understand trends and estimate properties before time consuming first-principles calculations. By introducing a

description of the surface energy via bond cutting we were able to understand the main surface energy contributions in Pmn2$_1$ Li$_2$FeSiO$_4$. This enabled us to determine the low energy surface compositions and estimate quantitatively their energy in order to find an appropriate set of surfaces that were studied by DFT. Introduction of an energy term that takes polarity compensation by charge transfer into account improved the fit quality significantly. We found that cutting through SiO$_4$ tetrahedra is most unfavorable, where cutting the first bond costs 2.7 eV which is four times higher than through Fe-O bonds. Li-O bonds are approximately only two thirds the Fe-O bond energy. The bond cutting energy values reflect the strong covalent Si-O bonds and indicate that in most environments the surface of Li$_2$FeSiO$_4$ will always exhibit unaltered SiO$_4$ tetrahedra.

Yet, not only do the strengths of Si-O bonds differ significantly from Fe-O and Li-O, but also do the elastic properties. We have shown that the general relaxation behavior of undercoordinated surface atoms is characterized by a movement towards the surface. Si however behaves fundamentally different from the others. In general the "directionality" of nearest-neighbor bonds seems much more pronounced for Si than for Fe and Li, which is reflected in the rigid antilinear behavior of bond-angle – bond-length variations for undercoordinated Si (see Fig. 7). Furthermore the response of the cation-O$_4$ tetrahedra in subsurface layers shows that FeO$_4$ and LiO$_4$ can be distorted easily whereas SiO$_4$ firstly is a near to perfectly symmetric tetrahedron and secondly is much more rigid, when it comes to bond angle and length change (see Fig. 6). This observation is closely related to the basic idea of introducing Si or P in Li electrode materials, whose principle purpose is to stabilize the crystal structure upon Li removal. In contrast to the redox active transition metal (TM) ions, Si stabilizes the crystal structure due to the strongly directional covalent bonds even under changing the adjacent chemical environment. Instead of the Li vacancy, it is here the surface that introduces this change. In contrast, the TM-O and Li-O bonds are less directional and supposably rather correspond to ionic bonds.

In addition, we determined the influence of correlation effects on the stability of the surfaces by comparing the results of GGA and GGA+U calculations. We found a consistent increase in energy (approx. 15 %), whenever undercoordinated Fe is involved. The influence on the Wulff shape, however, is marginal. It consists of {110}, {010} and {001} surfaces, whose lowest energy termination can be understood within our simple model based in bond-cutting and polarity compensation arguments.

Our findings shed new light on how relaxation behavior can be understood in complex materials with mixed iono-covalent bonds. Furthermore, we hope that the determined model parameters can be directly transferred to other crystal polymorphs of Li$_2$FeSiO$_4$, as the tetrahedral cation-O coordination holds and only their relative orientation and placement differs. This will be a starting point for surface that compare the surface energies of these different polymorphs. This is especially interesting as they were found to be very close in energy which might turn surface energies into a critical contribution to the stability of nano-crystallites.

[1] Zhong G, Li Y, Yan P, Liu Z, Xie M, Lin H (2010) J Phys Chem C 114:3693–3700
[2] Bao L, Gao W, Su Y, Wang Z, Li N, Chen S, Wu F (2013) Chin Sci Bull 78:575–584
[3] Arroyo-de Dompablo M, Armand M, Tarascon J, Amador U (2006) Electrochem Comm 8:1292–1298
[4] Kokalj A, Dominko R, Mali G, Meden A, Gaberscek M, Jamnik J (2007) Chem Mater 19:3633–3640
[5] Dominko R, Bele M, Gaberscek M, Meden A, Remskar M, Jamnik J (2006) Electrochem Comm 8:217–222
[6] Arroyo-deDompablo M, Dominko R, Gallardo-Amores J, Dupont L, Mali G, Ehrenberg H, Jamnik J, Moran E (2008) Chem Mater 20:5574–5584
[7] Arroyo y de Dompablo M, Gallardo-Amores J, García-Martínez J, Morán E, Tarascon JM, Armand M (2008) Solid State Ionics 179:1758–1762
[8] Nishimura Si, Hayase S, Kanno R, Yashima M, Nakayama N, Yamada A (2008) J Am Chem Soc 130:13212
[9] Saracibar A, Van der Ven A, Arroyo-de Dompablo ME (2012) Chem Mater 24:495–503
[10] Armstrong AR, Kuganathan N, Islam MS, Bruce PG (2011) J Am Chem Soc 133:13031
[11] Liivat A, Thomas JO (2011) Solid State Ionics 192:58–64
[12] Mali G, Sirisopanaporn C, Masquelier C, Hanzel D, Dominko R (2011) Chem Mater 23:2735–2744
[13] Sirisopanaporn C, Dominko R, Masquelier C, Armstrong AR, Mali G, Bruce PG (2011) J Mater Chem 21:17823
[14] Sirisopanaporn C, Masquelier C, Bruce PG, Armstrong AR, Dominko R (2011) J Am Chem Soc 133:1263–1265
[15] Nyten A, Kamali S, Haggstrom L, Gustafsson T, Thomas JO (2006) J Mater Chem 16:2266–2272
[16] Wang L, Zhou F, Meng Y, Ceder G (2007) Physical Review B 76:1–11
[17] Wang L, Zhou F, Ceder G (2008) Electrochem Solid-State Lett 11(6):A94–A96
[18] Park KS, Xiao P, Kim SY, Dylla A, Choi YM, Henkelman G, Stevenson KJ, Goodenough JB (2012) Chem Mater 24:3212–3218
[19] Chetty N, Martin RM (1992) Phys Rev B 45:6074–6088
[20] Reuter K, Scheffler M (2001) Phys Rev B 65:035406
[21] Groß A (2008) J Comput Theor Nanosci 5:894
[22] Rogal J, Reuter K (2007) Ab initio atomistic thermodynamics for surfaces: A primer. In: Experiment, Modeling and Simulation of Gas- Surface Interactions for Reactive Flows in Hypersonic Flights, pp (pp. 2–1 2–18). Educational Notes RTO–EN–AVT–142, Paper 2. Neuilly–sur–Seine

[23] Körmann F, Dick A, Hickel T, Neugebauer J (2011) Phys Rev B 83:165114

[24] Lorenz S, Scheffler M, Groß A (2006) Phys Rev B 73:115431

[25] Goniakowski J, Finocchi F, Noguera C (2008) Rep Prog Phys 71:016501

[26] Bertaut F (1958) Comptes Rendus 246:3447 – 3450

[27] Tasker PW (1979) J Phys C: Solid State Phys 12:4977

[28] Noguera C (2000) J Phys: Condens Matter 12:R367

[29] Wander A, Schedin F, Steadman P, Norris A, McGrath R, Turner T, Thornton G, Harrison N (2001) Phys Rev Lett 86:3811–3814

[30] Meyer B, Marx D (2003) Phys Rev B 67:035403

[31] Stengel M (2011) Phys Rev B 84:1–16

[32] Christensen A, Carter EA (1998) Phys Rev B 58:8050–8064

[33] Ong SP, Richards WD, Jain A, Hautier G, Kocher M, Cholia S, Gunter D, Chevrier VL, Persson KA, Ceder G (2013) Comp Mat Sci 68:314 – 319

[34] Kresse G, Furthmüller J (1996) Comp Mat Sci 6:15 – 50

[35] Kresse G, Furthmüller J (1996) Phys Rev B 54:11169–11186

[36] Perdew JP, Burke K, Wang Y (1996) Phys Rev B 54:16533–16539

[37] Dudarev SL, Botton GA, Savrasov SY, Humphreys CJ, Sutton AP (1998) Phys Rev B 57:1505–1509

[38] Lischka M, Mosch C, Groß A (2007) Electrochim Acta 52:2219

[39] Sakong S, Groß A (2007) J Phys Chem A 111:8814

[40] Leung K, Qi Y, Zavadil KR, Jung YS, Dillon AC, Cavanagh AS, Lee SH, George SM (2011) J Am Chem Soc 133:14741–14754

[41] Leung K (2013) J Phys Chem C 117(4):1539–1547

[42] Anisimov VI, Zaanen J, Andersen OK (1991) Phys Rev B 44:943–954

[43] Liechtenstein AI, Anisimov VI, Zaanen J (1995) Phys Rev B 52:R5467–R5470

[44] Stausholm-Moller J, Kristoffersen HH, Hinnemann B, Madsen GKH, Hammer B (2010) J Chem Phys 133:144708

[45] Zhou F, Cococcioni M, Marianetti CA, Morgan D, Ceder G (2004) Phys Rev B 70:235121

[46] Wang L, Maxisch T, Ceder G (2006) Phys Rev B 73:195107

[47] Blöchl PE (1994) Phys Rev B 50:17953–17979

[48] Kresse G, Joubert D (1999) Phys Rev B 59:1758–1775

[49] Larsson P, Ahuja R, Nyten A, Thomas JO (2006) Electrochem Comm 8:797 – 800

[50] Wu S, Zhu Z, Yang Y, Hou Z (2009) Comp Mat Sci 44:1243 – 1251

[51] Seo DH, Kim H, Park I, Hong J, Kang K (2011) Phys Rev B 84:220106

[52] Zhang P, Hu CH, Wu SQ, Zhu ZZ, Yang Y (2012) Phys Chem Chem Phys 14:7346–7351

[53] Neugebauer J, Scheffler M (1992) Phys Rev B 46:16067–16080

[54] Makov G, Payne MC (1995) Phys Rev B 51:4014–4022

[55] Bengtsson L (1999) Phys Rev B 59:12301–12304

[56] Momma K, Izumi F (2011) J Appl Crystal 44:1272–1276

[57] Riedel E (1999) Anorganische Chemie, 4th edn. De Gruyter, Berlin ; New York

[58] Hörmann N, Groß A (2013) Method, to be published

[59] Mulliken RS (1955) J Chem Phys 23:1833–1840

[60] Henkelman G, Arnaldsson A, Jonsson H (2006) Comp Mat Sci 36:354 – 360

[61] Groß A (2009) Theoretical Surface Science - A Microscopic Perspective. Springer

[62] Lischka M, Groß A (2002) Phys Rev B 65:075420